150.
Coduto, D. P., Yeung, M. C. & Kitch, W. A. (2011). *Geotechnical engineering. Principles and practices* (2nd ed.). Pearson.
Cousins, B. F. (1978). Stability charts for simple earth slopes. *Journal of the Geotechnical Engineering Division 104*(2), 267–279.
Das, B. M. & Sobhan, K. (2018). *Principles of Geotechnical Engineering* (9th ed.). Cengage.
Davis, R. O. & Selvadurai, A. P. (2005). *Plasticity and geomechanics*. Cambridge University Press.
Dawnson, E. M., Roth, W. H. & Drescher, A. (1999). Slope stability analysis by strength reduction. *Geotechnique 49*(6), 835–840.
Duncan, J. M. (1996). State of the art: limit equilibrium and finite-element analysis of slopes. *Journal of Geotechnical Engineering 122*(7), 577–596.
Duncan, J. M., Wright, S. G. & Brandon, T. L. (2014). *Soil Strength and slope stability*. John Wiley & Sons.
Fine Inc. (2016). *GEO5. Slope stability analysis software based on the limit equilibrium method*. Praha, Czech Republic.
Geo-Slope Inc. (2012). *SLOPE/W Version 2012. Slope stability analysis software based on the limit equilibrium method*. Calgary, Canada.
Griffiths, D. V. & Lane, P. A. (1999). Slope stability analysis by finite elements. *Geotechnique 49*(3), 387–403.
Hammah, R. E., Yacoub, T. E. & Curran, J. H. (2007). Serviceability-based slope factor of safety using the shear strength reduction (SSR) method. In L. R. e Sousa, C. Olalla, & N. Grossmann (Eds.), *Proceedings of the 11th Congress of the International Society for Rock Mechanics*, Lisbon.
Hoek, E. (2000). Personal communication.
Hoek, E. & Bray, J. (1974, 1977, 1981). *Rock slope engineering*. Institution of Mining and Metallurgy. London. (First, second and third editions, respectively).
Huang, Y. H. (2014). *Slope stability analysis by the limit equilibrium method. Fundamentals and methods*. American Society of Civil Engineers (ASCE) Press. Reston, Virginia.
Interactive Software Designs Inc. (2007). *XSTABL. Slope stability analysis software based on the limit equilibrium method*. Moscow, Idaho.
Itasca, Inc. (2016). *FLAC (Fast Lagrangian Analysis of Continua) Version 8.0*. Minneapolis, Minnesota: Itasca Consulting Group, Inc.
Janbu, N. (1954)a. Application of composite slip surfaces for stability analysis. In *European Conference on Stability of Earth Slopes.* Stockholm, Sweden, Volume 3, pp. 43–49.
Janbu, N. (1954)b. *Stability analysis of slopes with dimensionless parameters*. Thesis for the Doctor of Science in the Field of Civil Engineering. Harvard University, Soil Mechanics Series, No. 46.
Juang, C. H., Jhi, Y. Y. & Lee, D. H. (1998). Stability analysis of existing slopes considering uncertainty. *Engineering Geology 49*(2), 111–122.
Lacasse, S., Nadim, F., Liu, Z. Q., Eidsvig, U. K., Le, T. M. H. & Lin, C. G. (2019). Risk assessment and dams. Recent developments and applications. In *Proceedings of the XVII European Conference on Soil Mechanics and Geotechnical Engineering (ECSMGE-2019). Geotechnical Engineering foundation of the future.* Reykjavik, Iceland. September 2019.
Leshchinsky, B. (2013). Comparison of limit equilibrium and limit analysis for complex slopes. In *Geo-Congress 2013: Stability and Performance of Slopes and Embankments III*, pp. 1280–

1289.
Mesri, G. & Shahien, M. (2003). Residual shear strength mobilized in first-time slope failures. *J. Geotech. Geoenviron. ASCE 129*(1), 12–31.
Michalowski, R. L. (2002). Stability charts for uniform slopes. *J. Geotech. Geoenviron. ASCE 128-4*(GT9), 351–355.
Michalowski, R. L. (2013). Stability assessment of slopes with cracks using limit analysis. *Canadian Geotechnical Journal 50*, 1011–1021.
Microsoft (2016). *Excel Software. Version 2016*. Microsoft. Redmond, Washington.
Morgenstern, N. R. (1963). Stability charts for earth slopes during rapid drawdown. *Géotechnique 13*(1), 121–131.
Morgenstern, N. R. & Price, V. E. (1965). The analysis of the stability of general slip surfaces. *Géotechnique 15*(1), 77–93.
Mostyn, G. R. & Small, J. C. (1987). Methods of stability analysis. In B. F. Walker & R. Fell (Eds.), *Soil slope stability*, pp. 71–120. Balkema. Rotterdam.
O'Connor, M. J. & Mitchell, R. J. (1977). An extension of the Bishop and Morgenstern slope stability charts. *Canadian Geotechnical Journal 14*(1), 144–151.
Potts, D. M. & Zdravkovic, L. (1999). *Finite element analysis in geotechnical engineering. Theory*. Thomas Telford. London: Thomas Telford.
Rocscience Inc. (2015). *SLIDE Version 7. Slope stability analysis software based on the limit equilibrium method*. Toronto, Canada.
Scott, C. R. (1994). *An Introduction to Soil Mechanics and Foundations* (3rd ed.). Springer-Science & Business Media, B.V.
Spencer, E. (1967). A method of analysis of the stability of embankments assuming parallel interslice forces. *Géotechnique 17*, 11–26.
Spencer, E. (1973). Thrust line criterion in embankment stability analysis. *Géotechnique 23*, 85–100.
Steward, T., Sivakugan, N., Shukla, S. K. & Das, B. M. (2010). Taylor's slope stability charts revisited. *International Journal of Geomechanics 11*(4), 348–352.
Taylor, D. W. (1948). *Fundamentals of Soil Mechanics*. Wiley. New York.
Terzaghi, K., Peck, R. B. & Mesri, G. (1996). *Soil mechanics in engineering practice*. John Wiley & Sons.
Utili, S. (2013). Investigation by limit analysis on the stability of slopes with cracks. *Geotechnique 6*(2), 140–154.
Utili, S. & Abd, A. H. (2016). On the stability of fissured slopes subject to seismic action. *International Journal for Numerical and Analytical Methods in Geomechanics 40*, 785–806.
Vanmarcke, E. H. (1980). Probabilistic stability analysis of earth slopes. *Engineering Geology 16*(1-2), 29–50.
Verruijt, A. (2012). *Soil Mechanics*. Delft University of Technology, Delft, The Netherlands (Available for dowloading at http://geo.verruijt.net/).
Wang, L., Hwang, J., Juang, H. & Atamturktur, S. (2013). Reliability-based design of rock slopes. A new perspective on design robustness. *Engineering Geology 154*, 56–63.
Wyllie, D. C. (2018). *Rock slope engineering. Civil Applications* (5th ed.). CRC Press. Taylor & Francis.
Wyllie, D. C. & Mah, C. (2004). *Rock slope engineering. Civil and Mining* (4th ed.). CRC Press.
Yu, H. S., Salgado, R., Sloan, S. W. & Kim, J. M. (1998). Limit analysis versus limit equilibrium for slope stability. *J. Geotech. Geoenviron. ASCE 124*(1), 1–11.

Eisenhower Bridge North Abutment and Approach Settlement: A Case History of Timber Pile Downdrag and Comparative Downdrag Effect on Steel Piles

Steven J. Olson, P.E., M.ASCE[1]

[1]HDR, Minneapolis, MN. E-mail: steve.olson@hdrinc.com

ABSTRACT

The north abutment and approach of the Eisenhower Bridge has settled significantly since completion in 1960 and is currently several feet lower as compared to the 1960 construction plan profile. The north approach originally consisted of a 25-foot-high embankment placed on a soil profile of loose/soft alluvial sands, silts, and clays (alluvium) underlain by a very dense layer of sands and gravels; the north abutment was supported by 26 timber piles driven through the embankment fill and alluvium to practical refusal bearing on very dense sands and gravels. Given the timber piles were driven to practical refusal in competent materials, the movement in the abutment appears to be a result of downdrag loads. As the approach embankment adjacent to the abutment settled from consolidation of the soft alluvium, drag load developed on the timber piles and induced excessive internal stress and end bearing pressure on the piles. It is believed the yield strength of the timber piles was exceeded in compression resulting in damaged or broken piles. The purpose of this study is to demonstrate how the drag loads on the timber pile foundation system caused excessive stress and movement of the abutment and provide comparative analyses to model the effect if steel piles had been selected in place of the timber piles.

INTRODUCTION

The Minnesota Department of Transportation (MnDOT) Bridge No. 9040 (Wisconsin Department of Transportation Bridge No. B-47-24), referred to as the Eisenhower Bridge, is currently under replacement as MnDOT Bridge No. 25033. The new bridge will be located just upstream of the existing Eisenhower Bridge (see Figure 1) on Truck Highway No. 63 (TH 63) between Red Wing, Minnesota, and Hager City, Wisconsin.

SITE GEOLOGY

At Red Wing, the geologic profile consists of bedrock near the surface (within 5 to 10 feet) of elevation 720 feet. The surficial soils consist of alluvial sand, gravel and sandstone colluvium. The bedrock nearest the surface and exposed at the south abutment is the St. Lawrence Formation, which consists of intermixed siltstone and sandstone with some dolomitic zones. Underlying the St. Lawrence Formation is the Franconia Formation that is variably glauconitic, fine to medium grained sandstone with seams of shale, and zones where sandstone is cemented with dolomite.

The bedrock surface is deeper north of Red Wing within the Mississippi River Valley and heading into Wisconsin; it ranges from 85 feet to more than 145 feet below ground/water surface, varying from approximately elevation 588 feet to 537 feet at the north abutment.

The south abutment at Red Wing is supported on a spread footing bearing on the St. Lawrence Formation. Pier 1 is supported on driven H-piles through sandy alluvium with piles bearing on the underlying sandstone. Piers 2 through 7, and the north abutment and approach of the Eisenhower Bridge, are located within the Mississippi River Valley in Pierce County, Wisconsin. The Normal Pool Elevation of the Mississippi River is 666.64 feet at Red Wing. The river valley is relatively low in elevation (about elevation 670 feet) and therefore required an approach embankment with a height well over 25 feet (to elevation 695 feet) placed to support the north abutment. The north abutment and approach act as a causeway over a seasonal floodplain and have settled since original bridge completion in 1960. Figure 2 shows how the existing abutment and approach is currently several feet lower as compared to the 1960 plan profile provided by MnDOT.

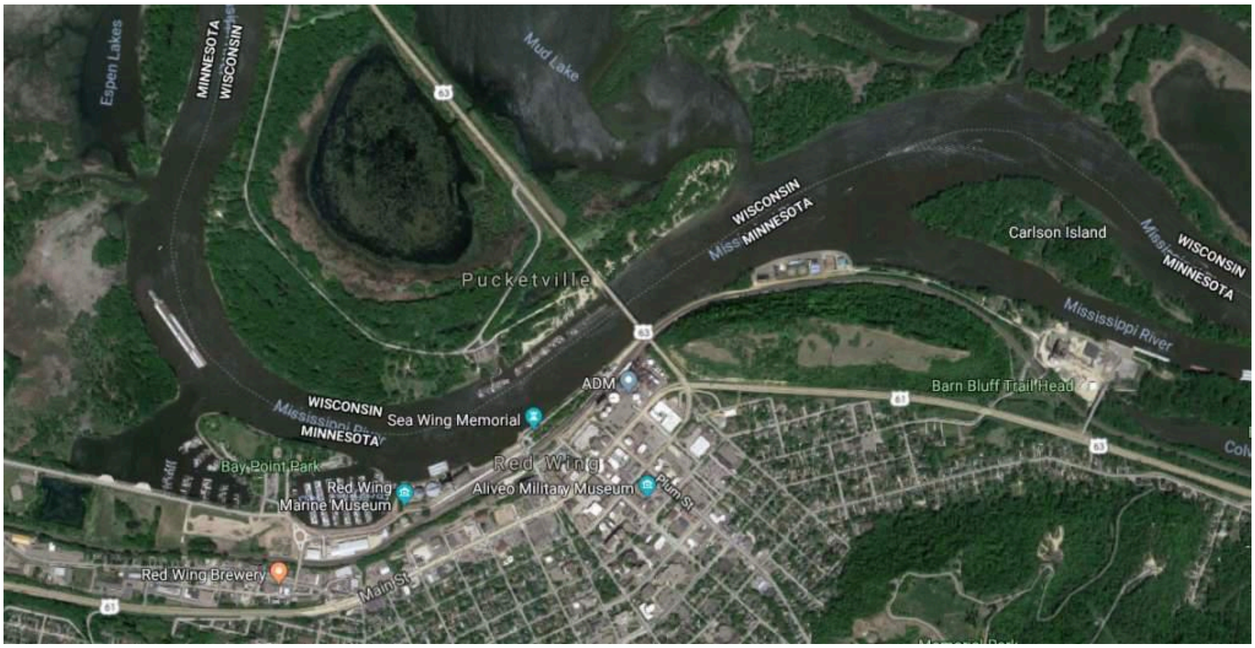

Figure 1. The aerial view shows the existing Eisenhower Bridge.

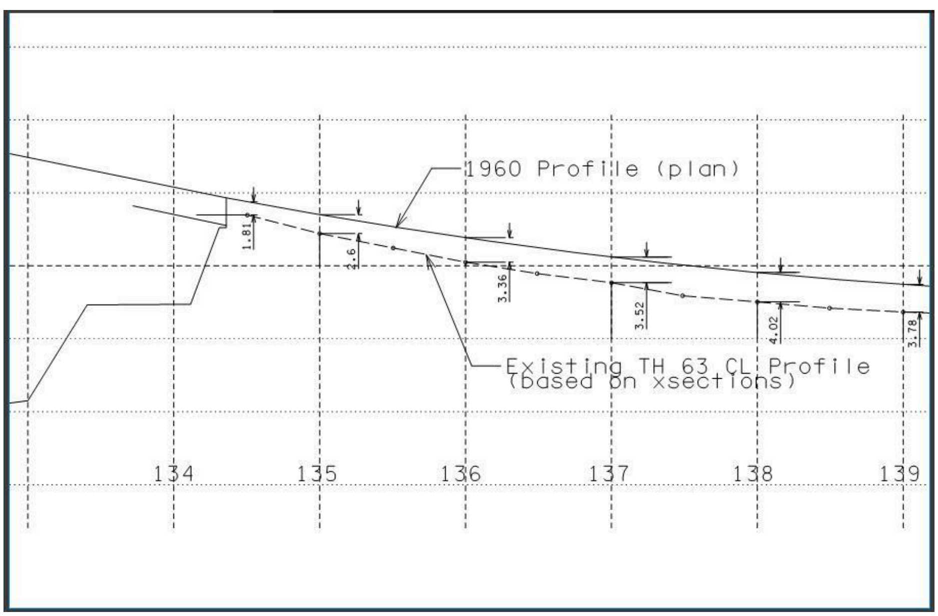

Figure 2. Comparison of existing TH 63 profile to 1960 plan profile

SUBSURFACE PROFILE

Prior to placement of the north approach embankment for the Eisenhower Bridge beginning in April 1959, the subsurface profile (based on boring T-1) from surface elevation 666 feet consisted of 9 feet of very soft native silts/clays, and then 12 feet of loose sands, underlain by more than 50 feet of soft, compressible clay, overlying very dense gravels with sands. Boring T-1 terminated within the gravel/sand layer. Young's Modulus of the very dense gravel/sand layer was conservatively estimated at 20 kips per square inch with Standard Penetration Test (N60) values of 50 blows per 0.5 feet.

Deeper exploration in 2014 (boring T-109) revealed the very dense gravel/sand layer supporting the timber piles to be about 10 feet thick and is underlain by medium dense coarse sands that extend to sandstone bedrock of the Franconia Formation at elevation 537 feet. See Wisconsin side (right hand side) of Figure 3 from MnDOT Memo (2014).

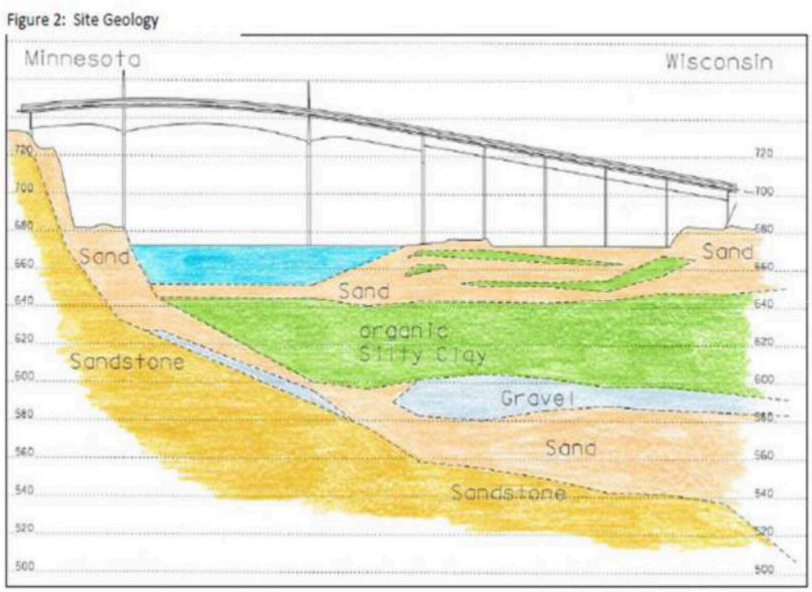

Figure 3. Subsurface profile along the bridge alignment

BRIDGE FOUNDATION CONSTRUCTION

The north bridge abutment and approach embankment was placed during the summer of 1959 to about final elevation 695 feet. Soon after embankment placement, the north abutment piles were installed in December of 1959. The abutment foundation system consisted of 26 timber piles driven with a Vulcan 1-M steam hammer. The hammer has a ram weight of 5,000 pounds and available stroke of 3 feet for maximum rated strike energy of 15,000 feet-pounds.

The timber piles were generally 105 feet long and driven to an average length of 97 feet below cutoff elevation at 689.95 feet. The measured pile diameter averaged about 15 inches at the pile top and 7 inches at the base. The piles were driven to practical refusal at an average set of 0.08 inches per blow (equivalent to 150 bpf). The timber piles extended about 2-3 feet into the very dense sands and gravels to an average pile base elevation at 593 feet.

Based on the Engineering News Record (ENR) formula, the piles were driven to an average bearing resistance of 101.6 tons (203 kips) per pile. The minimum required installation bearing resistance was 20 tons per pile and calculated dead load plus overturning was 16 tons per pile, as indicated on the plan document notes. Therefore, the piles were installed with an average safety factor of 5.0 or more in axial bearing support based on resistance at end of drive.

EMBANKMENT SETTLEMENT

The abutment and approach embankment construction required well over 25 feet of fill bearing on the native alluvial river valley soils at the north abutment location. The weight of this fill has induced vertical movement of the north approach as a result of long-term consolidation settlement of the compressible alluvial soils, especially the 50-feet-thick layer of soft silty clay loam immediately above the very dense loamy sands and gravels on which the timber piles are bearing. To estimate the embankment settlement, the consolidation test results (Figure 4) from MnDOT Memo (2014) were utilized.

Table 1: Consolidation Test Results (average values from T110)

Moisture Content	56%
Over Consolidation Ratio	0.8
Initial Void Ratio, e_0	1.5
C_c	0.63
C_r	0.06
C_v (ft^2/day)	0.13

Figure 4. Consolidation test results

Estimated embankment settlement was calculated to be about 50 inches over duration on the order of 50 years.

DEFINITIONS

The following definitions are applicable and important in understanding the pile analysis results:

Base Resistance — the resistance or support from soil or bedrock at the pile base as a result of pile movement. If there is no pile end movement, there is no base resistance (i.e., friction pile). If moderate pile movement, pile is supported in both side resistance and base resistance. If excessive pile movement, base resistance may be very high.

Downdrag — the movement of the pile as a result of soil movement when the neutral plane is located above or within a zone of compressible soil.

Negative Side Resistance — soil load (drag load) applied from the top portion of the pile in a downward direction with respect to the pile.

Neutral Plane — the location or zone along the pile at transition or interface between positive and negative side resistance. It is also the location or zone along the pile where the pile and adjacent soil move together. In addition, it is the location of maximum stress within the pile.

Positive Side Resistance — soil support from the bottom portion of the pile in an upward direction with respect to the pile.

Side Resistance — resistance or support of the pile from soil adjacent to the pile perimeter that is applied to the pile in either direction, up (positive support) or down (drag load).

PILE ANALYSIS RESULTS

Neutral Plane methodology as described in Section 7.2.1.3.4 of FHWA-NHI-16-009 (2016) was used to show the effect of downdrag on a single pile. Four models were developed, each showing a condition in time after final bridge construction. The first model represents the condition immediately after final bridge completion.

The second model represents a point in time when full side resistance was engaged. This model includes the assumption of full side resistance with no pile base resistance; the assumption is supported by Section 4.1.2 of Tomlinson and Woodward (2008) that shows the effects of loading a pile. Figure 10.8.2.2.2-1 in AASHTO (2017) suggests that the majority of side resistance in cohesive soil is mobilized after only 0.6% of the base diameter of the pile, in this case, about 0.05 inch settlement; Figure 10.8.2.2.2-4 indicates very little (~15% or less) base resistance would have mobilized at that amount of settlement.

The third model represents the mobilization of full-side resistance and full-base resistance.

The final model represents the condition at complete pile downdrag movement.

Since side resistance is mobilized with less movement than pile base resistance, it is first mobilized before pile base resistance. Beginning immediately after pile installation, the pile load consists of the pile's own weight, which is supported entirely in side resistance. Side resistance is believed to be the primary means of support at the initial load condition as supported by Tomlinson and Woodward (2008).

As the dead load of the new bridge is applied during construction, the dead load is supported primarily in side resistance as shown in Figure 5. Drag load is 19 kips resulting in a maximum pile load of about 54 kips, which is well below the 187 kips available (based on pile diameter) at the neutral plane. At this condition, the neutral plane is located about 12 feet below the top of pile. Because the neutral is above the compressible layer, additional pile movement occurred during consolidation of the compressible clay layer.

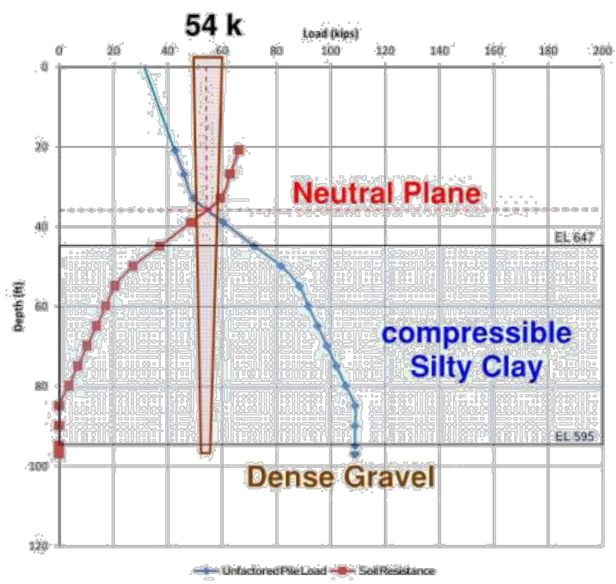

Figure 5. First model – Immediately after bridge construction

With additional consolidation, all available side resistance is mobilized (101 kips) as shown in Figure 6. The neutral plane location moved downward to 40 feet below the pile top. This resulted in less structural pile resistance (66 kips) due to the smaller diameter of the tapered timber pile. At this stage, the maximum pile load is 69 kips, greater than the available compressive resistance of the pile.

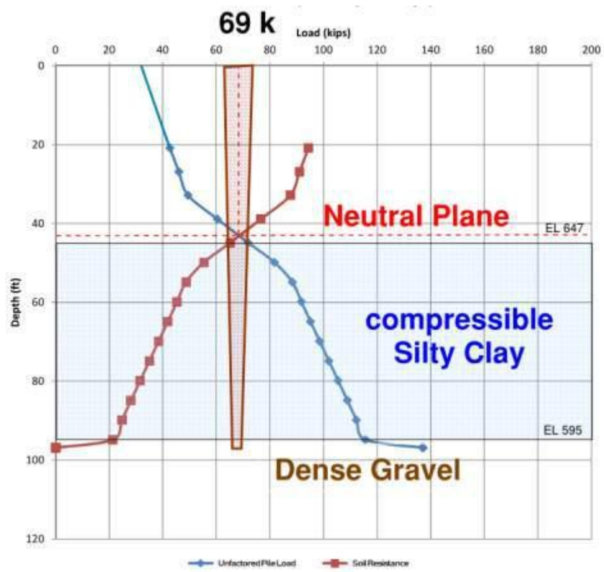

Figure 6. Second model – after additional consolidation of compressible layer

The next model includes full available side resistance. Due to continued consolidation, full pile base resistance is mobilized as well as shown in Figure 7. Now the side resistance is 101 kips and base resistance is 54 kips. The drag load is almost double the dead load at 60 kips. The increased drag load caused the internal pile load (95 kips) to exceed the available structural resistance in compression. The pile base resistance is at 54 kips, resulting in base stress very near the compressive strength of timber (1.25 ksi). The neutral plane was moved downward with additional consolidation of the compressible clay layer, now at 66 feet below the top of pile. At 66 feet, the neutral plane is about the midpoint of the compressible clay layer.

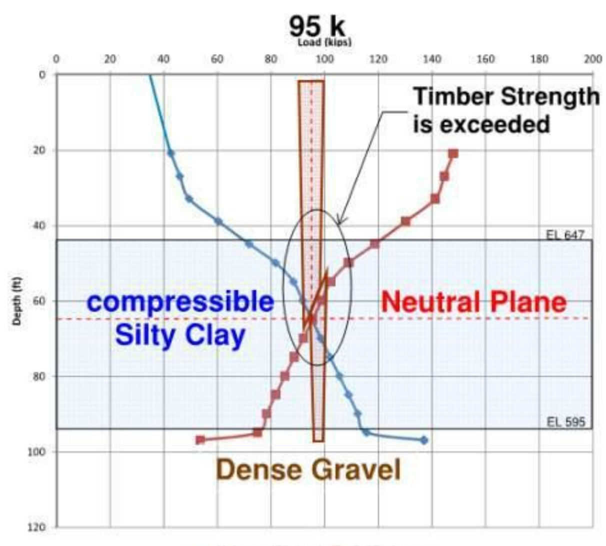

Figure 7. Third model – after full-side resistance and full-base resistance

The final model was performed with neutral plane located at the bottom of the compressible layer at completion of pile downdrag movement as shown in Figure 8. At this location, maximum pile load is 116 kips and pile base load is 95 kips — both are well above the structural capacity of the timber pile. Pile stress is 2.6 ksi and 2.2 ksi at the neutral plane and pile base, respectively, greatly exceeding 1.25 ksi, the strength of timber pile in compression.

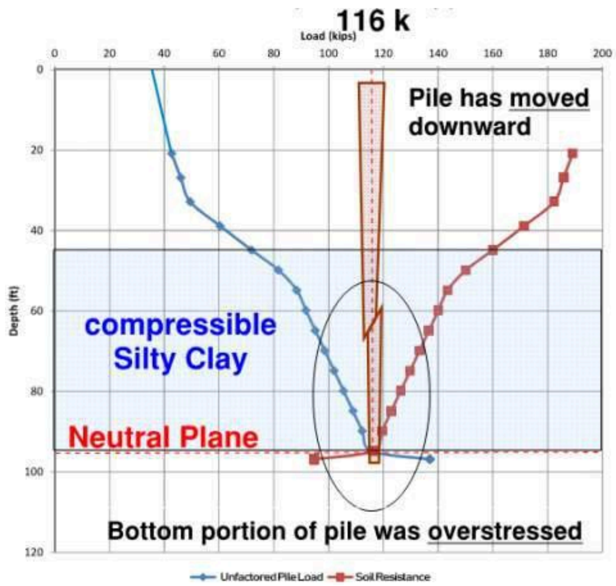

Figure 8. Final model – at completion of pile downdrag

As shown in Figure 7, the timber strength is exceeded around the midpoint of the compressible clay layer. Therefore, the portion of pile below the midpoint of the clay layer could no longer be considered to provide axial geotechnical resistance since it is broken structurally. Consequently, it is anticipated the abutment will move as a result of reduced axial resistance of the piles.

Given the movement of the system is driven by structural failure of the timber piles, steel piles which typically have higher yield strengths and a consistent area along the length, were analyzed. For the initial comparison, a similar sized 7-inch diameter closed-end steel pipe pile was modeled with the downdrag condition where the neutral plane is located at the bottom of the compressible layer. The maximum pile load was 98 kips and pile base load was 88 kips. Pipe pile stress was about 18 ksi and 2 ksi at the neutral plane and pile base, respectively. Since the yield strength of Grade 2 steel is 35 ksi, the pipe pile strength in compression would have supported the dead load and additional dragload.

Another comparison of similar sized steel H-pile was modeled at the downdrag condition. An HP 8x36 was modeled with the neutral plane located at the bottom of the compressible layer. The maximum pile load was 82 kips and pile base load was 75 kips. H-pile compressive stress was about 8 ksi and 7 ksi at the neutral plane and pile base, respectively, well below the compressive strength of steel.

Table 1 shows the comparison of three pile types each modeled with the neutral plane at the bottom of compressible soil layer. The results indicate the timber pile has been overstressed and pile top has moved downward from excessive drag load on the pile during consolidation of the compressible soil layer, resulting in the phenomenon known as pile downdrag.

Due to the higher strength in compression of steel as compared to timber, neither the pipe pile nor the H-pile would have been overstressed. Compressive stress at the pipe pile base would have been similar to the timber pile, at approximately 2 ksi. The compressive stress at the base of the H-pile would have been slightly higher at 7 ksi. The very dense gravels at the pile base have a Young's Modulus estimated at about 20 ksi, so movement at the base of either steel pipe or H-pile would have been minimal. Therefore, the pile top would have remained very near the constructed position and pile downdrag movement would not have been realized with the use of the same number and length of steel piles driven to bear on the very dense gravel layer.

Table 1. Comparison of Pile Types and Compressive Stress

Pile Type	Compressive Stress at Neutral Plane (ksi)	Compressive Stress at Pile Base (ksi)	Pile Compressive Strength	Notes
Timber	2.6	2.2	1.25 ksi	NG, stress exceeds timber strength
7” diameter Closed-end Pipe	18	2	35 ksi	Ok, stress less than steel strength
HP 8x36	8	7	35 ksi	Ok, stress less than steel strength

SUMMARY AND CONCLUSIONS

Timber pile strength was exceeded due to high drag load on the piles. In the author’s opinion, this resulted in damaged and broken timber piles that happened over time with pile downdrag movement. Alternatively, the steel pipe piles or H-piles were able to structurally support the increased stress from pile drag load without pile failure in compression since these piles have higher allowable stresses and a more consistent cross-section with depth.

This case history demonstrates piles should be checked for structural capacity (strength limit state) based on the dead load plus maximum projected drag load. The maximum drag load will occur with the neutral plane modeled at the bottom of the lowest compressible layer and should be accounted for in the structural evaluation of the pile.

Embankment movement (settlement) is independent of pile type and would have occurred as a result of embankment settlement due to the weight of the fill consolidating the compressible layer over time, in this case about 50 years. Timber pile bases were assumed to be generally restricted from movement as the modulus of the gravel layer is much greater than calculated stress at the pile base. For the top of timber piles to move 1.8 feet (Figure 2) or more with restricted base movement supports the inference that timber piles were damaged and most likely sheared in compression parallel to timber grain during pile downdrag movement.

In comparison, steel piles would have withstood the compressive stress at the neutral plane without pile damage. Additionally, the compressive stress at the pile base is relatively small, even for the H-pile, as compared to the modulus of gravel in compression. Therefore, most likely steel piles would also have been restricted from movement and penetration into the gravel layer. Without significant pile base penetration into the gravel and with steel strength sufficient to support the dead load plus additional dragload, the steel piles would likely have supported the abutment as the embankment fill beneath the abutment and the approach settled over time. Effectively, this may have resulted in a void developing beneath the abutment and probably several pavement overlays over the years to maintain grade at the abutment and approach